A Study on the Cypress Viaduct Collapse and Seismic Performance of a Retrofitted Bent

Hajime Ohuchi　　Takashi Matsuda
Yozo Goto

サイプレス高架橋の倒壊と補強後の耐震性に関する一考察

大内　一　　松田　隆
後藤洋三

概　要

1989年ロマプリエタ地震でのサイプレス高架橋の被災と，補強後橋脚の耐震性を数値解析により検討した。橋脚の破壊と損傷程度は，地盤条件と橋脚構造タイプに深い因果関係を持つと予想され，最初の解析はその一連のシナリオに定量的説明を加えることを目的とする。また第2の解析は補強後橋脚の合衆国現行設計レベルの地震に対する耐震性を検討することを目的とする。数値解析は，有効入力地震動を予測するための ① 地盤の応答解析と，② 地盤－基礎相互作用解析，③ 復元力モデルのための橋脚の FEM 非線形解析，および ④ これらを総合した橋脚の非線形応答解析の4つのフェーズに分けて実施した。その結果次のことが合理的に予測出来た：① 重複反射理論による地震動の増幅，② FEM 非線形解析による既存橋脚および耐震補強後橋脚の破壊と強度，③ 橋脚の非線形応答解析による地盤条件と橋脚タイプの違いによる破壊性状，および補強後橋脚の現設計レベル地震に対する十分な耐震性。

Abstract

This paper describes numerical studies on the bent collapse of the Cypress Viaduct during the Loma Prieta Earthquake and on the seismic performance of the same type of retrofitted bent. The purpose of the first simulation is to identify seismic behavior of collapsed and surviving bents due to ground conditions and structural types and that of the second simulation to estimate seismic performance against several earthquakes consistent with the current U. S. design standard. Systematized analyses consist of the followings : ① dynamic response of ground, ② soil-foundation dynamic interaction, ③ nonlinear static behavior of bent, and ④ nonlinear dynamic response of bent. These analytical results provided following conclusions. ① Amplified seismic motion on the surface ground was predicted based on the multiple reflection theory. ② Finite element nonlinear analyses provided good agreement with test results both of pre-retrofitted and retrofitted bents. ③ Nonlinear dynamic response analyses provided a quantitative explanation on the relationships between ground conditions, bent types, and bent collapses and also ensured sufficient seismic safety of the retrofitted bent.

1. Introduction

Catastrophic collapse of the Cypress Viaduct at Loma Prieta Earthquake 1989, caused 41 fatalities and amount of economic losses in San Francisco Bay area. A great concern was concentrated on the engineering issue to be resolved with 48 bent collapses in the 1.2 km long part of I-880 at the Cypress section. In the U.S., comprehensive seismic design specification was provided after the 1971 San Fernando Earthquake. However a great number of bridges including the Cypress Viaduct, were constructed in 1950's and 1960's. As the results, seismic vulnerability of existing bridges and seismic strengthening method were urged to investigate and a number of experimental and analytical studies have been conducted including field tests with survived bents. In these backgrounds, this paper presents numerical simulation studies on the collapse of the Cypress Viaduct and on the seismic performance of the retrofitted bent against several earthquakes consistent with the current U. S. seismic design guideline. A rational prediction of the Cypress Viaduct collapse is believed to contribute in the future earthquake hazard mitigation practice. Also a prediction on the seismic performance of the retrofitted bent may provide effective information in promoting seismic strengthening program for similar type viaduct in California.

2. General

2.1 Damage Summary

As reported in the JSCE Reconnaissance Report on the Loma Prieta Earthquake of Oct. 17, 1989[1], the cause of bent damages is considered as deeply related with the underlying ground condition and the structure type. The Cypress north side section was on reclaimed soft soil, while the south side section on dense silty sand. In the north side, all the upper decks fell down onto lower decks except one span portion. On the other hand in the south side falling down of upper decks was prevented except about 150 m portion next to the north side.

The bent types are conceptually categolized into 3 structure types as shown in Fig. 1 due to location of pinned joint and bent-cap structural type, i. e. reinforced or prestressed concrete. B type bent was employed in many parts and all collapsed in the north side. Among five A type bents existed in the north side, two of them survived despite significant damages suffered. In the south end of north side, all the C type bents also collapsed.

2.2 Objectives of Present Study

Numerical simulations are classified into two phases, i. e. collapse simulation of existed bents and seismic performance simulation of a retrofitted bent as shown in Fig. 2.

The objective of 1st simulation is to provide rational answer to the following two questions: Are bent collapse in the north side section and bent survival in the south side section predicted if considering different ground conditions? and do B and C type bents collapse and an A Type bent not collapse in the north side section?. As shown in Fig. 2, analytical studies for this simulation consist of 4 parts: Ⅰ dynamic response analysis of ground, Ⅱ soil-foundation dynamic interaction analysis, Ⅲ static nonlinear-analysis of bent and Ⅳ nonlinear dynamic response analysis of bent. The objective of 2 nd simulation is to provide similar rational answer to the following question: how much structural margin does retrofitted bent possess against earthquakes with the accelera-

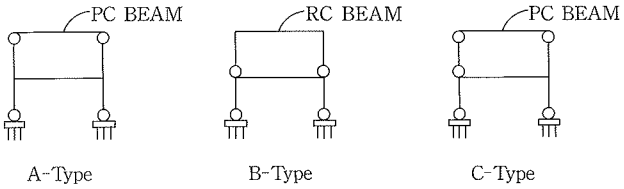

Fig. 1 Bent Type-Conceptual Structure

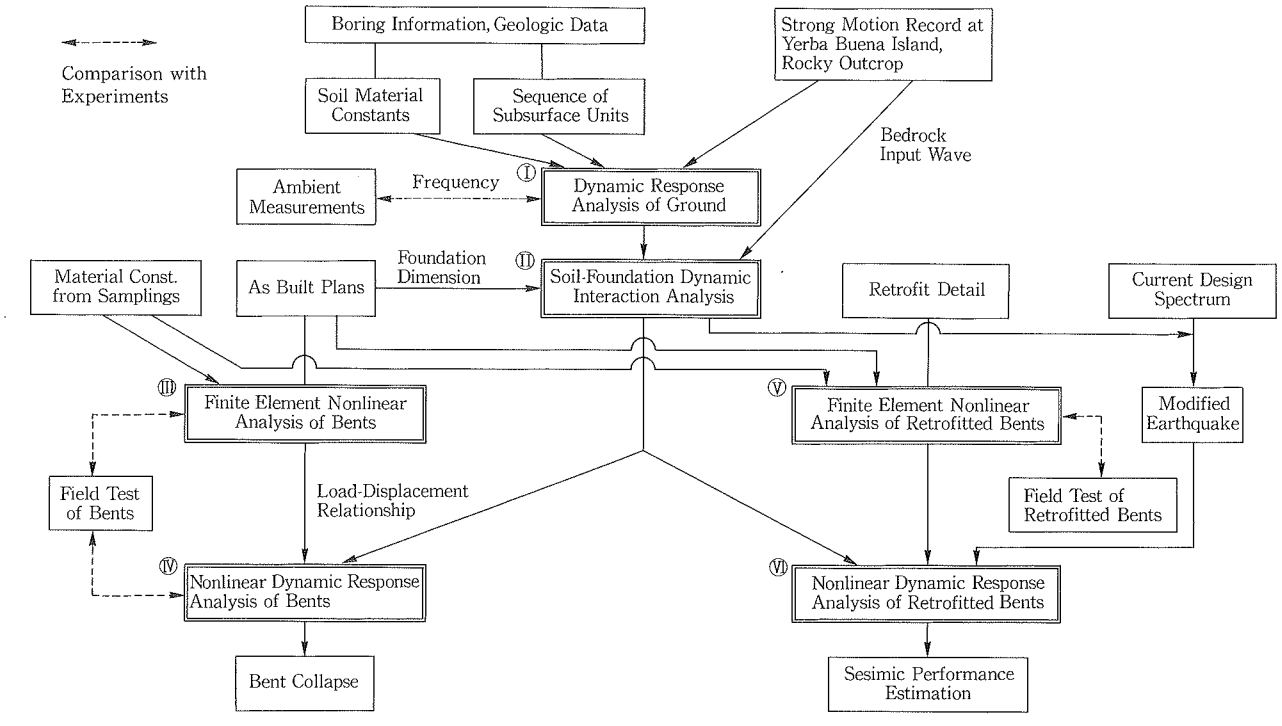

Fig. 2 Analytical Study Procedure

tion amplitude consistent with the current seismic design standard? As shown in Fig. 2, analytical studies for this simulation consist of two parts: Ⓥ Static nonlinear analysis of retrofitted bent and Ⓥ Nonlinear dynamic response analysis of retrofitted bent. Results from part I and II analyses are also utilized as an input motion and foundation characteristics for the part Ⓥ dynamic response analyses. From the damage observation of survived bent and from the available accelerogram observed in the nearby site, the transverse motion of bridge axis is considered as dominant. Accordingly, all the above analyses are carried out against transverse motion of bridge axis neglecting structural contribution from the members parallel to the bridge longitudinal axis such as box girders except their gravity load.

3. Collapse Simulations

3.1 Dynamic Response of Ground

3.1.1 Analytical Method A dynamic response analysis of a multi-layered ground is conducted based on the multiple reflection theory. The equivalent linear method is utilized to consider nonlinear behavior of soil material[3] becasuse of comparatively small input acceleration of 0.035 G from bedrock. Soil layers in the north side and the south side sections are modelled on the basis of boring log datas[2] and PS velocity logging datas.[4),5),6)] A significant difference appears from the surface to 16.5 m depth below ground line (G.L.), i. e. soft bay mud from 2 to 6 m depth in the north side while dense silty sand from 4.5 to 16.5 m depth in the south side. An accelerogram recorded at Yerba Buena Island, rocky outcrop about 7 km distant from the Cypress section (EW : 0.067 G, NS : 0.029 G) is employed as an input wave from bedrock. This island consists of Franciscan formation identical to the bedrock of the Cypress section. A half of EW component, is utilized as the incident wave from bedrock.

3.1.2 Analytical Results Fig. 3 illustrates the calculated transfer function between bedrock and ground surface, in which the first natural period predicted is respectively 0.61 and 0.68 Hz in each side and its amplification factor is nearly equal to each other, however the amplification in the higher frequency region (1 Hz~4 Hz) is larger in the north side than in the south side. The analytical period agrees fairly well with the measured value of 0.7 Hz in the ambient vibration[7]. Fig. 4 illustrates the calculated ground surface acceleration waves with maximum accelerations of 194 gal in the north side and of 135 gal

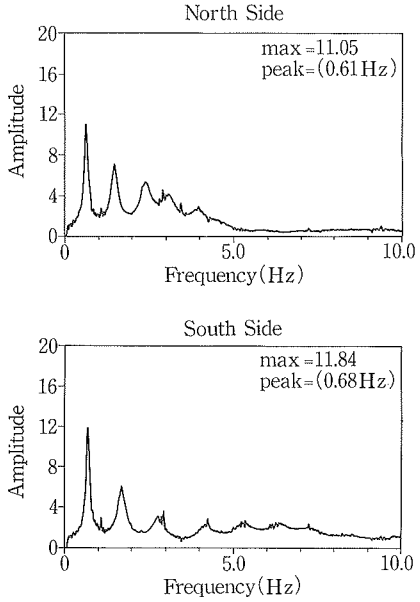

Fig. 3 Calculated Transfer Function Between Bedrock and Ground Surface

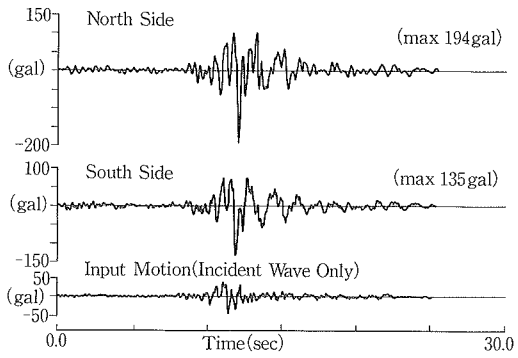

Fig. 4 Ground Surface Acceleration Based on Multiple Reflection Theory

Table. 1 Dynamic Characteristics of Ground

Layer No.	North Side					South Side				
	Thickness (m)	S-Wave*1 Velocity (m/sec)	Dynamic Soil Properties after ELM*2 Convergence: Shear Modulus (tf/m²)	Damping Ratio (%)	Shear Strain (10^{-4})	Thickness (m)	S-Wave*1 Velocity (m/sec)	Dynamic Soil Properties after ELM*2 Convergence: Shear Modulus (tf/m²)	Damping Ratio (%)	Shear Strain (10^{-4})
1	2.1	150	3,950	3.3	0.7	4.0	200	7,180	2.9	0.5
2	4.2	80	870	8.0	11.7	2.9	250	10,800	3.7	0.9
3	8.7	229	9,900	4.8	1.9	10.0	350	21,200	3.7	0.9
4	9.0	80	9,720	5.4	2.9	10.0	350	20,000	4.9	1.5
5	9.5	80	9,450	5.7	3.6	10.0	226	9,700	5.7	4.3
6	9.5	80	11,100	5.5	3.5	15.5	226	10,700	5.8	4.6
7	12.5	350	21,200	6.1	2.4	16.5	372	23,900	5.8	2.2
8	12.5	350	20,600	6.7	3.0	17.5	372	23,600	6.3	2.6
9	14.0	350	20,100	7.3	3.5	17.0	372	22,700	7.3	3.5
10	13.5	512	47,500	4.9	1.5	19.0	518	47,600	5.3	1.8
11	14.0	512	47,300	4.9	1.5	20.5	518	47,500	5.3	1.8
12	9.5	300	12,700	9.8	5.7	21.5	604	67,000	4.6	1.4
13	18.0	543	53,500	4.8	1.5	18.0	604	66,200	5.0	1.6
14	18.0	543	52,900	5.1	1.6	—	—	—	—	—
15	18.5	543	52,600	5.2	1.7	—	—	—	—	—

*1 Eualuated by N-value[2]
*2 ELM : Equivalent Linear Method

in the south side. Calculated dynamic characteristics of the ground are tabulated in Table. 1.

3.2 Soil-Foundation Dynamic Interaction

3.2.1 Analytical Method As a pair of bent columns stand on the independent foundation with each other, a unit of pile cap-pile foundation system is idealized. Representative analytical bents to be discussed in this paper are No.96, 85 and 71 for A, B and C type bent respectively. The dynamic response under forced vibration is calculated[8] with using the axsymmetric finite element model as shown in Fig. 5. The material characteristics of ground layers such as shear stiffness and damping are provided by the results obtained in the previous ground response analysis. The nonlinear behavior such as slip between soil and foundation is neglected because no ground surface cracks suggesting significant slip were observed in the post-earthquake field investigation.

3.2.2 Analytical Results The spring stiffness and effective input acceleration are evaluated on the top of pile cap. Fig. 6 illustrates frequency dependent characteristics of the spring analytically obtained from load-displacement relationship under horizontal harmonic excitation at the pile top. The real part corresponds to stiffness while the imaginary part damping characteristics. The spring stiffness in the south side provides about 3.5 times that in the north side. Obtained effective input acceleration is shown in Fig. 7.

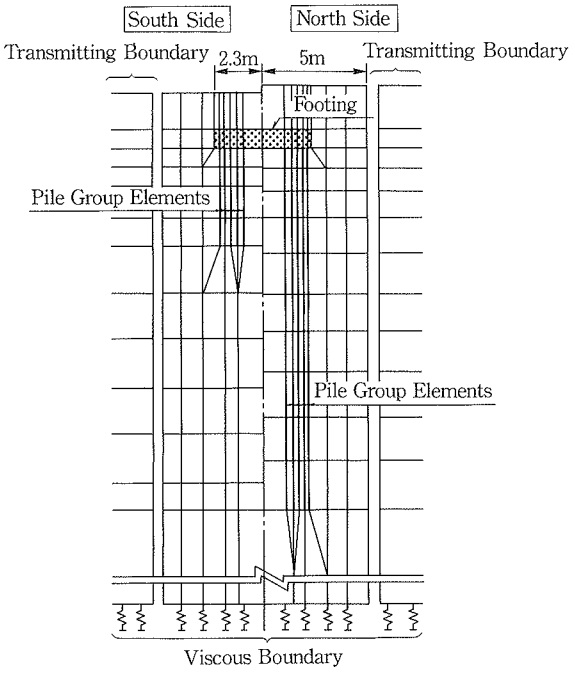

Fig. 5 Axsymmetric Finite Element Models for Interaction Analysis

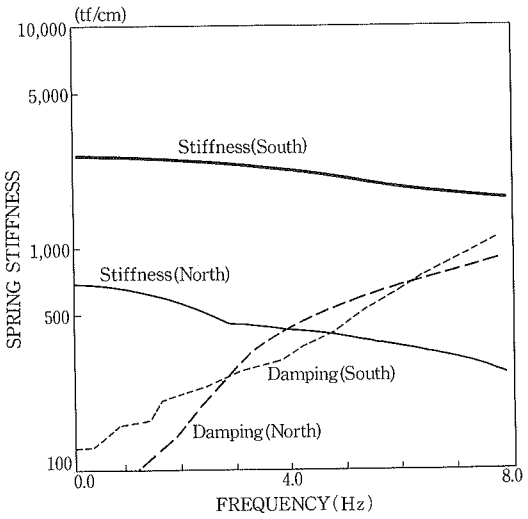

Fig. 6 Frequency Dependent Characteristics of Spring

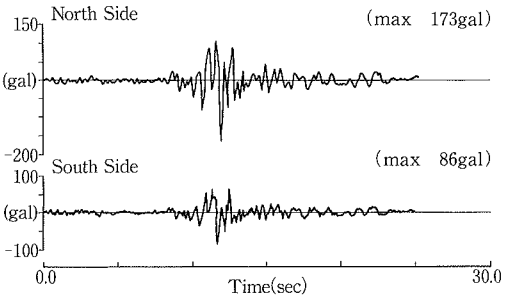

Fig. 7 Effective Ground Surface Acceleration (on the Pile Cap)

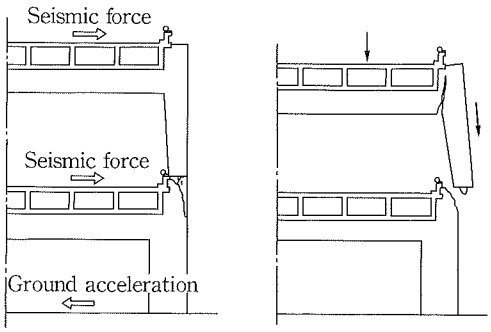

Fig. 8 (a) Typical Failure Sequence of a B Type Bent (Ref. 9)

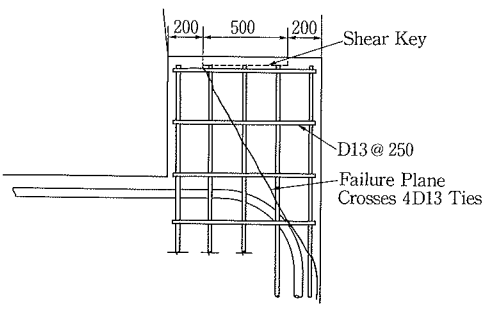

Fig. 8 (b) A Shear Crack along Bent Down Rebar in The Joint (Ref. 9)

3.3 Static Nonlinear Behavior of Bents

A typical bent failure sequence[9] and an critical shear crack along bent down rebar in the joint are illustrated in Fig. 8 (a) and (b). The objectives in this section are to predict this critical shear failure and load-displacement relationships for the nonlinear dynamic response analysis in the following section. Caltrans conducted horizontal loading tests[10] to estimate ultimate loading capacity of the existing bent (undestructive test) and to investigate seismic performance of the retrofitted bent (destructive test) with using the survived bents No. 45-47 categorized as B type in the present study. The accuracy of present analyses will be verified through comparison with this nondestructive test result.

3.3.1 Analytical Method The finite element nonlinear analysis program 'ABAQUS[12]'is utilized combined with the separate subroutine for concrete constitutive law[13]. Material constants are assumed as follows on the basis of the sampling test results and design informations[10]: for concrete, $f_c'=443\ kgf/cm^2$, $f_t=7.5\sqrt{6300}\ psi=595\ psi=42\ kgf/cm^2$, $E_c=2.8\times10^5\ kgf/cm^2$ and for steel reinforcement, $f_y=3032\ kgf/cm^2$ (Grade 40 steel), $E_s=2\times10^6\ kgf/cm^2$. The case of concrete tensile strength of $f_t=60\ kgf/cm^2$ is additionally analized to discuss the effect of material constant variation on the nonlinear behavior.

After applying dead load, i. e. weight of bent caps and one span length box girder, static horizontal load uniformly distributed in each bent cap is incrementally increased. A horizontal load distribution on the height, i. e. the ratio, of P_2 to P_1 is determined based on the elastic first mode. Fig. 9 illustrates dimension and steel reinforcement arrangements of the representative bent (B type)[14]. The upper and the lower concrete through shear key are assumed as monolithically connected except those through fiber board. No damage suffered in the past is assumed with all bents.

3.3.2 Analytical Results An ultimate crack pattern of B type bent is illustrated in Fig. 10. Even during dead load application, the shear crack initiates in the pedestal below the pinned joint of upper column

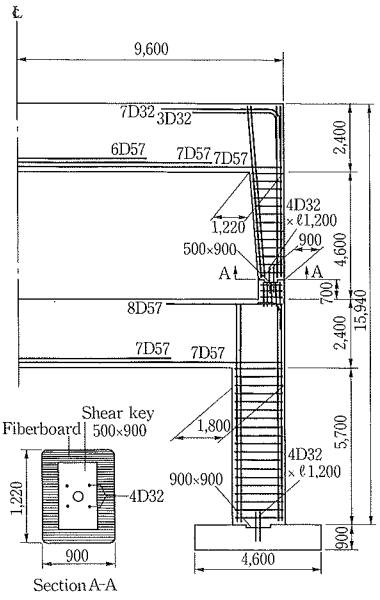

Fig. 9 Dimention and Reinforcement Detail of B Type Bent-No. 88 (Ref. 14)

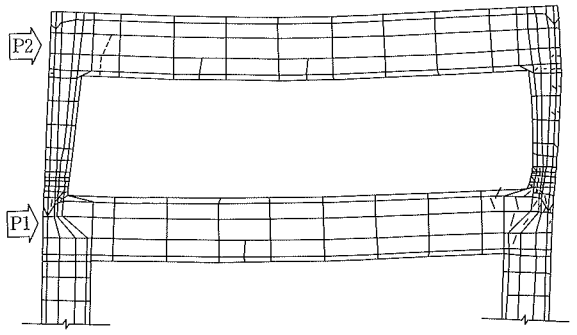

Fig. 10 Crack Pattern at Final Stage (B Type Bent)

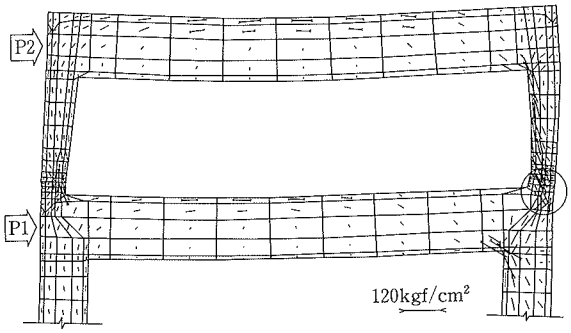

Fig. 11 Principal Compressive Stress Flow (B Type Bent)

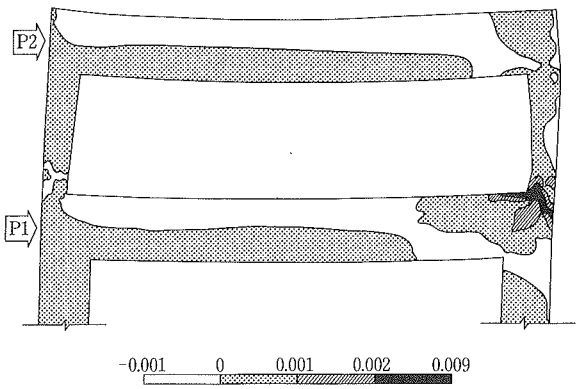

Fig. 12 Horizontal Strain ε_x Contour at Ultimate Stage (B Type Bent)

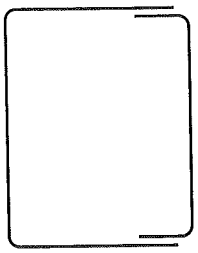

Fig. 13 Configuration of Transverse Reinforcement in the Joint Region

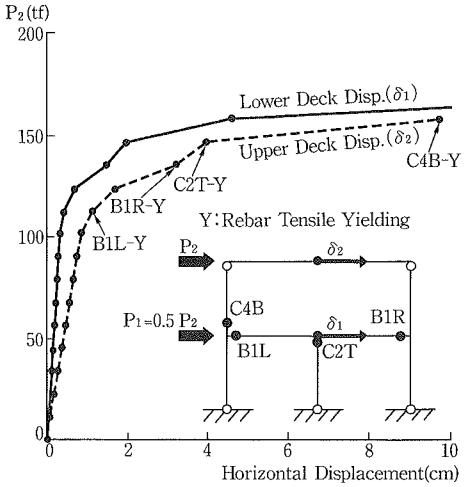

Fig. 14 Load-Displacement Relationship (A Type Bent)

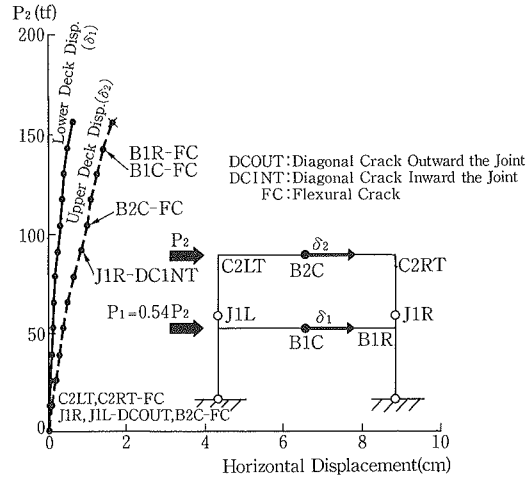

Fig. 15 Load-Displacement Relationship (B Type Bent)

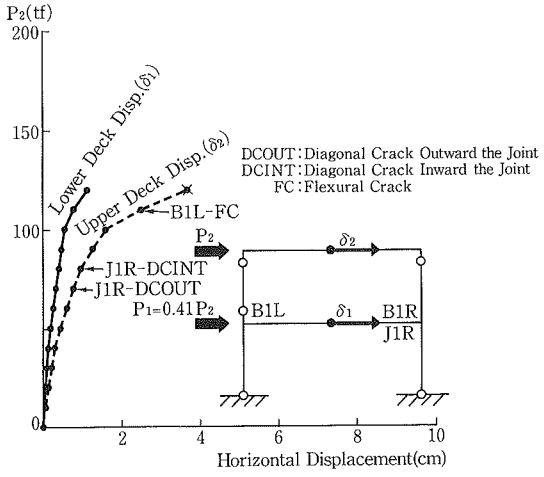

Fig. 16 Load-Displacement Relationship (C Type Bent)

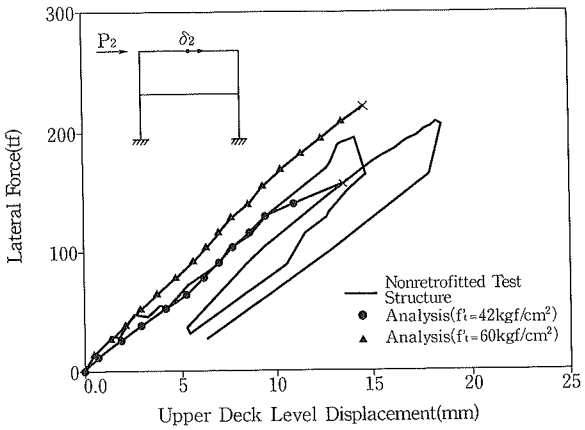

Fig. 17 Load-Displacement Relationship (Bent No. 46)

due to shear force outward the joint. With horizontal load increasing, this crack propagates diagonally along bent down rebar in the joint and then vertically into concrete outer-coverage, which corresponds the failure mode illustrated in Fig. 8 (b). The significant compressive stresses, as shown in Fig. 11, are transmitted vertically in the column inner side and rapidly change their direction into diagonal in the joint, that suggests the kick-out failure of the column base. The left end of upper bent cap is critical in flexural crack shown as the broken line in Fig. 10, which suggest the flexural crack concentration at upper bent cap end as shown in Fig. 8 (a) when considerng insufficieint anchorage of D 57 (No. 18) lower straight reinforcement (see Fig. 9) and bond depression under cyclic horizontal load. Fig. 12 illustrates horizontal strain contour of ε_x at ultimate stage in which the strain concentration in the joint is to be comparable to the failure surface of Fig. 8 (b). When additionally considering less and insufficient shear reinforcement, i. e. tied hoop utilized as shown in Fig. 13, this type of shear failure must be likely encouraged.

Horizontal load-displacement relationships for A, B and C type bents are respectively shown in Figs. 14 to 16. As shown in Fig. 14, the analytical result predicts flexural yielding type failure in the A type bent. In the B type bent, after the joint shear cracks extend to the concrete coverage, most of shear reinforcement in the pedestal ultimately yield. In the C

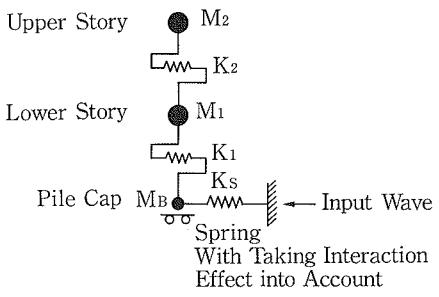

Fig. 18 Three Degrees of Freedom System Model for Nonlinear Dynamic Response

Table. 2 Natural Frequency of Bents

Structure Type	Site	Frequency(Hz)	
		1st	2nd
A Type	North Side	2.07	4.99
(No.96)	South Side	2.16	5.21
B Type	North Side	2.40	5.60
(No.88)	South Side	2.55	6.25
		(2.50)*	(6.50)*
C Type	North Side	2.17	5.54
(No.71)	South Side	2.31	5.71

( )* : Forced Vibration Test Results

Table. 3 Comparison of Upper Bent Responses Between North Side and South Side Input Motions

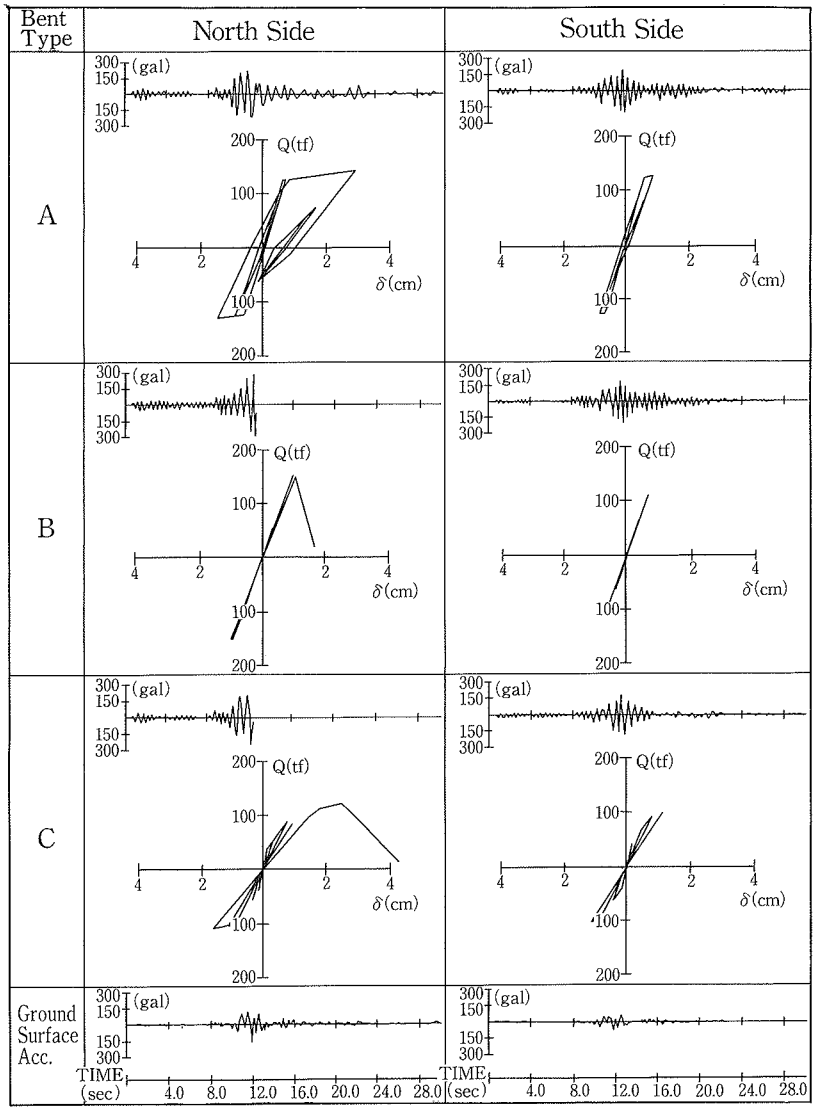

type bent with pinned joints at both upper column tops, the shear crack initiates from pedestal to joint at relatively high horizontal load. However because one of upper columns resists no horizontal load, the lateral shear force concentrates on the other column, resulting in lower ultimate loading capacity and lower lateral stiffness obtained rather than the B type bent.

The ultimate loading capacity of the B or C type bent is numerically determined by the load level when the internal lateral shear force in the critical column rapidly decrease umbalancing with the external horizontal load.

3.3.3 Comparison with Undestructive Test Results

In the field loading test, the horizontal load was applied only at the upper bent cap. Fig. 17 illustrates load-displacement relationship where the analytical result (f_t=42 kgf/cm²) agrees with experimental result in the ascending part. The predicted ultimate loading capacity is 156 tf in comparison with 210 tf in the experiment[10]. Because ultimate load is deeply dependent on shear cracks in the joint, the case with concrete tensile strength of f_t=60 kgf/cm² is alternatively analized to discuss its influence. The larger but more approximate ultimate loading capacity with 234 tf is obtained for this case. The stiffness difference between f_t=42 and 60 kgf/cm² cases depends on the difference of crack growth especially during dead load application. When considering possible initial crack existence in the experimental bent, the tensile strength between these values may be more reasonable to use. However because of better approximation in stiffness, the case of f_t=42 kgf/cm² is employed in all the following analyses.

3.4 Nonlinear Dynamic Response of Bents

3.4.1 Analytical Method Nonlinear dynamic response analyses are conducted with using three degrees of freedom systems including a spring taking soil-foundation interaction effect into account as shown in Fig. 18. As for the idealized enveloping curve for hysteresis models, shear force-relative displacements obtained from the finite element nonlinear analyses are idealized into tri-linear type model. As for the hysteretic rule, the flexural-failure-type degrading stiffness response model, so called Takeda model[15] is utilized for both upper and lower stories of the A type bent. In the B and C type bents, the similar model is utilized for the lower story while the origin-orient hysteresis model for the upper story failed in brittle shear. Based on the dynamic interaction analysis in the section 3. 2, the spring characteristics at base (Fig. 18) is idealized as a linear elastic model with damping calculated considering strain energy for radiation damping. Superstructure damping is assumed as of 3%.

3.4.2 Analytical Results Table. 2 shows elastic natural frequencies obtained from the three degrees of freedom system analyses. The analytical 1st natural frequency of 2.55 Hz agrees well with the forced vibration test result of 2.5 Hz.[9] for the B type bent. The obtained acceleration time histories and shear force-relative displacement hystresis in the critical upper story are tabulated in Table. 3 in which characteristic responses can be identified due to bent types and ground conditions. In the north side B and C type bents, the upper story collapses immeadiately after the maximum ground surface acceleration. On the other hand in the south side, both type bents survive with some stiffness reduction appearance. The A type bent in the north side does not collapse with hysteretic damping effect due to flexural yielding. This analytical performance ensures survival of actual No. 95 and No. 96 bents despite considerable damages observed. It is considered that flexural yielding type hysteresis characteristics significantly contribute on preventing bent from catastrophic collapse.

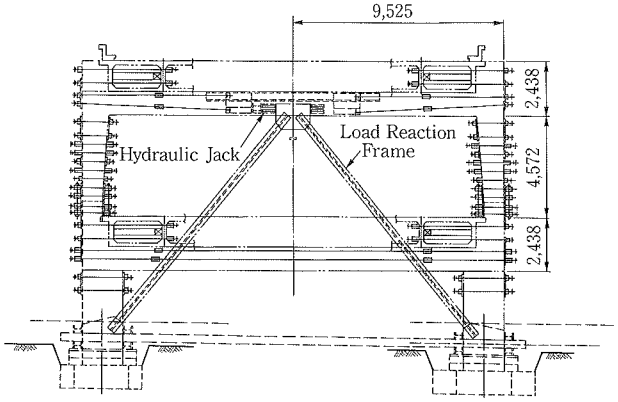

Fig. 19 Retrofit Detail (Bent No. 46)

4. Seismic Performance Simulation of Retrofitted Bents

4.1 Static Nonlinear Behavior of Retrofitted Bents

As described in the section 3. 3, Caltrans conducted horizontal loading tests of retrofitted bents using survived No. 45 to No. 47 bents with less damages[10]. After comparison with this destructive test results to verify the accuracy, the analytical results for the following dynamic response analysis are to be discussed.

4.1.1 Analytical Method The retrofitted No. 46 bent [16] (Fig. 19), presently categorized as B type bent is analized in this chapter. The jacking forces with prestressing rods (ϕ25 mm, ϕ35 mm for column confinement and ϕ35 mm for bent cap flexural strengthening) are modelled by a pair of nodal forces and diagonal rock bolts in the beam column joint is modelled as one of reinforcements. A Grade 40 steel is assumed for rock bolts and steel tubings to be combined with prestressing rods for column confinement.

Inadequate and insufficient anchorage of the bent cap lower reinforcement (D 57) as described in the section 3. 3. 2 should be considered. The insufficient anchorage directed depression is modelled by reducing yielding strength of D 57 rebar in the joints from f_{sy}= 3,023 kgf/cm^2 to $f_{sy}=f_{slip}$=1,890 kgf/cm^2 based on the pull-out test results[17] which provided the developed tensile stress-bar size relationship of reinforcing bar. Material constants and another assumption in the analysis are similar with those provided in the section 3. 3.

4.1.2 Analytical Results A comparison between experimental and analytical load-displacement relationship in the destructive test is shown in Fig. 20 to represent good approximation of a finite element nonlinear analysis. Analytical result in general ensure flexural type failure with fairly good agreement with experimental results.

Analytical load-displacement relationships, which are to be idealized for the hysteresis model in the following dynamic response analysis, are shown in Fig. 21. The analytical bent is the same as that

compared with destructive test result. The locations of yield hinges produced are also completely same as that. However, they appear in about 10% earlier horizontal load stage because of loadings imposed on both upper and lower bent caps.

4.2 Design Response Spectrum and Input Motion

Fig. 22 illustrates elastic acceleration response spectrums by the previously predicted acceleration wave on the Cypress north side and the representative acceleration records in the past. The elastic seismic response spectrums for three soil types specified in the seismic design guidline[18] are also shown. Design response fitted waves are respectively produced for 3 soil types by modifying acceleration amplitude of these waves with its phase angle unchanged.

4.3 Nonlinear Dynamic Response of Retrofitted Bents

4.3.1 Analytical Method A three degrees of freedom system is modelled for the Cypress wave and the modified Cypress wave, while a two degrees of freedom system is modelled for another three modified waves because foundation and ground condition are not identified. The Takeda Model with tri-linear type enveloping is also idealized for both upper and lower hysteresis characteristics in shear force-relative displacement relationship.

4.3.2 Analytical Results Analytical results are represented in Fig. 23. For the original Cypress wave, both upper and lower story responses remain in elastic. Except this case, the shear force reaches beyond elastic limit but not beyond yielding for any cases. The maximum response and the seismic performance evaluation in strength and ductility are provided in Table. 4 for each input motion respectively, where the ultimate strength and the ultimate displacement are temporarily defined by the yielding shear force Q_y and the relative displacement δ_u when concrete crush initiates at the upper story column top respectively. For all input waves, sufficient safety factor is assured in both strength and ductility. These results indicate that if the present type bent is strengthened in shear so that flexural-yielding-type performance be assured, sufficient margin in seismic performance can be provided against not only the Loma Prieta earthquake but the input motions consistent with the current seismic design guideline as well.

5. Concluding Remarks

Based on the results presented, a number of conclusions can be summarized in the followings.

① The two dimensional finite element analyses

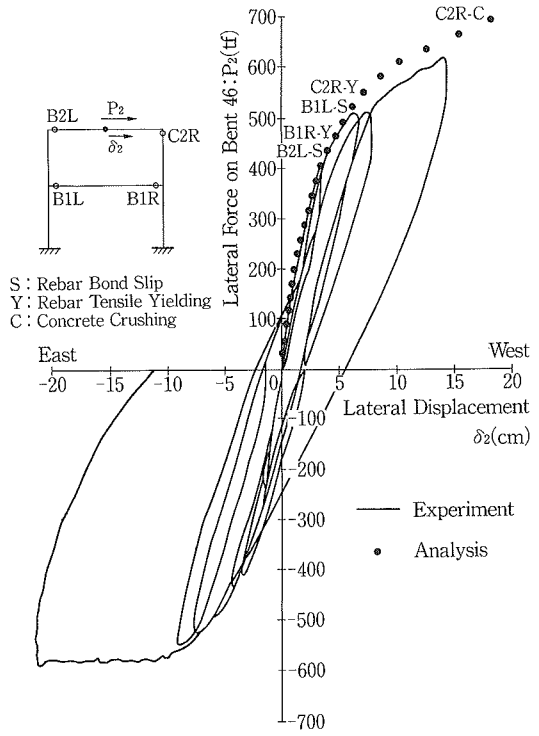

Fig. 20 Load-Displacement Relationship (Retrofitted Bent No. 46)

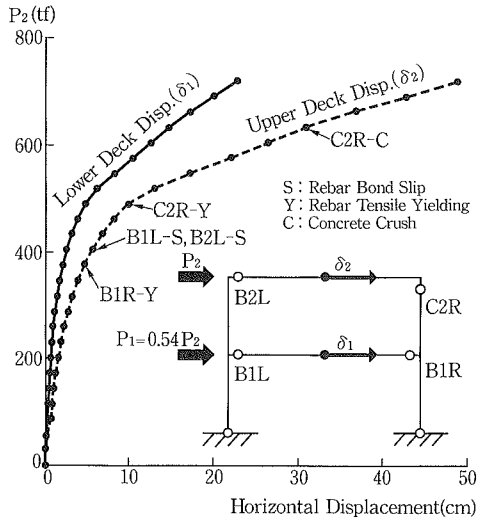

Fig. 21 Load-Displacemet Relationship (Retrofitted B Type Bent)

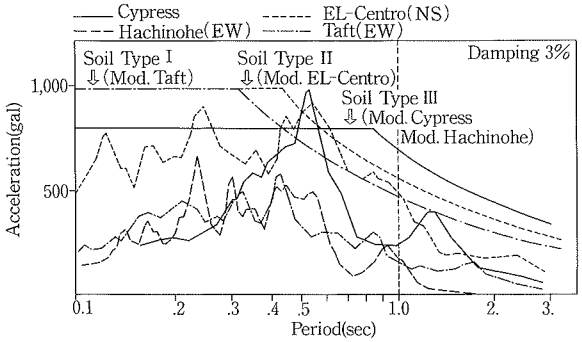

Fig. 22 Elastic Acceleration Spectrum

Table. 4 Seismic Performance of Retrofitted Bent

Input Earthquake	Story	Input		Response			Safety Factor	
		$\dot{y}_{o\,max}$ Max. Vel. (cm/sec)	$\ddot{y}_{o\,max}$ Max. Acc. (gal)	$(\ddot{y}_o+\ddot{\delta})_{max}$ Max. Acc. (gal)	δ_{max} Max. Disp (cm)	Q_{max} Max. Shear Force(tf)	Q_y/Q_{max} Strength	δ_u/δ_{max} Ductility
Cypress	2	24	173	398	1.00	222	2.23	16.30
	1			221	0.51	352	2.13	———
M. Cypress	2	68	345	635	2.33	349	1.42	7.00
	1			397	1.28	527	1.42	———
M. Hachinohe	2	49	310	680	2.84	383	1.29	5.74
	1			481	1.75	567	1.32	———
M. EL-Centro	2	47	383	810	3.65	437	1.13	4.47
	1			685	1.80	571	1.31	———
M. Taft	2	52	386	729	3.04	396	1.25	5.36
	1			491	1.52	547	1.37	———

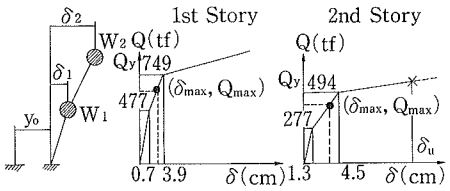

predicted nonlinear behaviors of the existed bents and of the retrofitted bent up to the failure with good agreements in comparison with experimental results.

The analyses of existed B and C type bents predicted final shear failure from the pedestal to the bent cap-column joint with yielding of insufficient shear reinforcement and also suggested flexural crack concentration at the end of second story bent cap due to inadequate anchorage length of. longitudinal reinforcement, those of which corresponds with the damages observed in the site.

On the other hand, the analysis of retrofitted bent provided good agreement with experimental results, especially taking the effect of insufficient anchorage length of longitudinal reinforcement of bent cap into account by temporarily idealizing its yield strength reduced.

② The multi degrees of freedom system nonlinear response analysis, on the basis of systematized analyses, i. e. on the amplified ground motion, on the soil-foundation interaction and on the nonlinear behavior of the bents up to the ultimate, provided rational explanation for the sequential collapse scenario of the Cypress Viaduct.

With good correspondence to the damages observed in the site, it was predicted that an a type bent in the north side survived due to its ductile flexural yielding behavior and both B and C type bents in the north side collapsed in shear, while those in the south side survived due to little less amplified ground motion.

For the dificiency of observed acceleration records in the Cypress Section, it can not directly verify the accuracy of the calculated

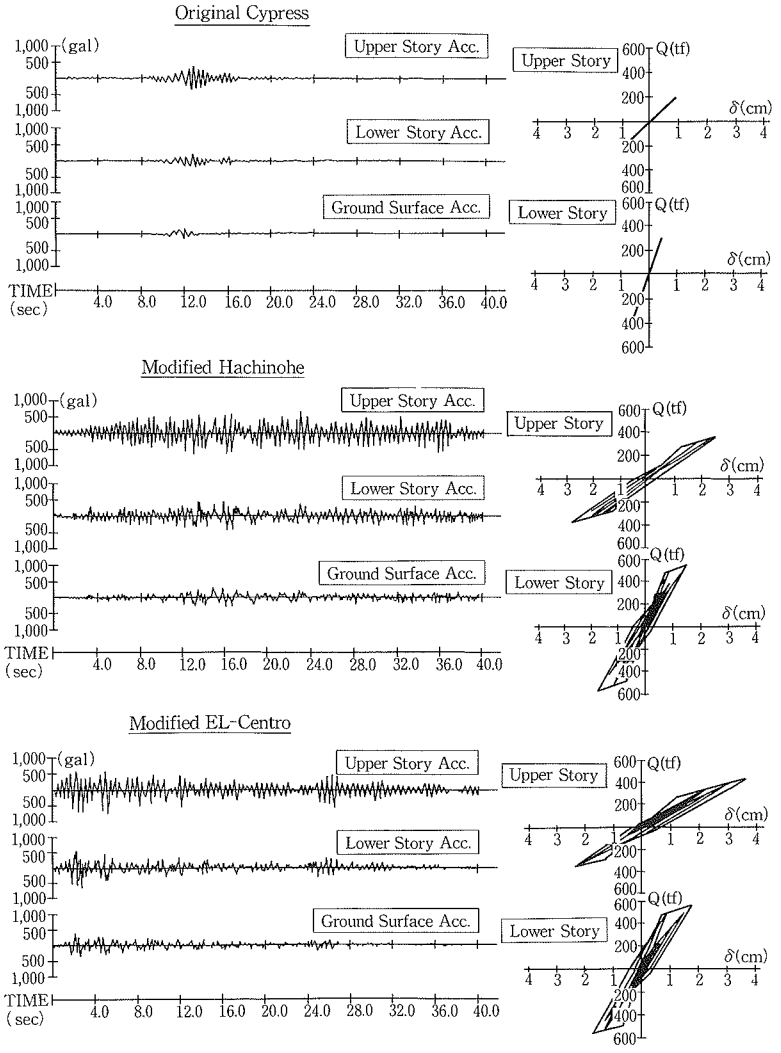

Fig. 23 Seismic Response of Retrofitted Bent (B Type)-Acceleration Time History and Shear Force-Relative Displacement Relationship

ground motion in the present procedure. However, it should be noted that the different damages of bents between the north and the south sides were appropriately lead due to the different input motions predicted. Namely, the present procedure with considering SH wave input, nonlinear material characteristics of soils and soil-foundatdon interaction, would be effective to provide a precise effective input motion for a simplified dynamic interaction model.

③ The present type of bent retrofitted mainly in shear provides sufficient seismic performance against input motions with acceleration amplitude consistent with the current seismic design guideline.

④ The collapse of the Cypress Viaduct is unlikely to provide effective lessons to the current seismic design practice in Japan because of the unusual structural feature with less redundancy and inadequate and insufficient reinforcement detail. In recent years, neverthless, a number of existing bridges with inadequate reinforcement such as cut-off reinforcing bars in column mid-section, are urged to be strengthened even in Japan. The present study hopefully suggests one of sophisticated method to evaluate seismic resistance of these existing structures with higher accuracy.

Acknowledgement

Most of informations and references utilized in the present study are from California Department of Transportation, United States Geological Survey and University of California. Especially, Prof. Idriss, University of California, Davis provided the geologic datas of the site. This paper is appreciably published in responding for their providing useful materials. Dr. Eto, Mr. Ejiri and Mr. Naganuma are appreciated for their consulting work through this project work.

We hope this paper will provide one of useful materials for seismic hazard mitigation practice.

References

1) The Earthquake Engineering Committee: Reconaissance report on the Loma Prieta Earthquake of Oct. 17, 1989, 2. 2 Analysis on the Damage Features of the Cypress Viaduct Caused by the Loma Prieta Earthquake of 1989, Proc. JSCE, Vol. 422/I-14, (Oct. 1990)

2) Caltrans: Log of Test Boring Concerning Cypress Viaduct

3) Kokusho T.: Dynamic Soil Properties and Nonlinear Seismic Response of Ground, (1983)

4) Caltrans: Borehole Velocity Surveys at the Embarcadero in San Francisco and the Cypress Structure in Oakland, (Aug. 1990)

5) Seed, H. B., et al.: Implication of Site Effects in the Mexico City Earthquake of Sept. 1985 for Earthquake Resistant Design Criteria in the San Fransisco Bay Area of California, UCB/EERC /03, (Mar. 1989)

6) Helly E. J. et al.: Flatland Deposits of the San Francisco Bay Region, California- Their Geology and Engineering Properties and Their Importance to Comprehensive Planning, Geological Survey Professional Paper 943

7) Ohmachi T. et al.: Ground Motion Characteristics in the San Francisco Bay Area Detected by Microtremor Measurements-A Preliminary Assesments-Tokyo Institute of Technology No. 800104, (Nov, 30. 1989)

8) Goto Y. et al.: On an Earthquake Analysis Method of Liquid-Structure-Ground Coupled System, Report of the Technical Research Inst. of Obayashi, No. 27, (1983)

9) Nims, D. K. et al.: Collapse of the Cypress Street Viaduct as a Result of the Loma Prieta Earthquake, UCB/EERC-89/16, (Nov. 1989)

10) Moehle, J. P. and Mahin, S. A.: Implications of Nondestructive and Destructive Tests on the Cypress Street Viaduct Structure, 7 th US-Japan Workshop on Bridge Structure, UJNR, (May. 1990)

11) Housner, G. W. et al.: Competing Against Time, Report to Governor George Deukmejian from the Governor's Board of Inquiry on the 1989 Loma Prieta Earthquake, (May. 1990)

12) Hibbit, Karlsson and Sorensen, Inc.: ABAQUS Theory Manual, Version 4. 6, (1987)

13) Naganuma K.: Final User's Manual (Version 7), Technical Research Institute, Obayashi Co. Ltd.

14) Caltrans: As Built Plans,10th to Distribution Structures, (July 26. 1957)

15) Takeda, T. et al.: Reinforced Concrete Response to Simulated Earthquakes, Jour. Structural Div., ASCE, Vol. 96, No. ST12, p. 2557～2573, (1970)

16) Caltrans: Cypress Street Viaduct Bent 45, 46 and 47 Retrofit Detail-As Built Drawing, (Dec. 1989)

17) Park, R. and Paulay, T.: Reinforced Concrete Structures, John Wiley & Sons, p. 407～410, (1975)

18) Applied Technology Council: Seismic Design Guideline for Highway Bridges, 2nd Printing, (June 1986)